doi:10.1016/j.jmb.2008.04.030 *J. Mol. Biol.* (2008) **381**, 73–88

JMB

Available online at www.sciencedirect.com

ScienceDirect

ELSEVIER

Selectional and Mutational Scope of Peptides Sequestering the Jun–Fos Coiled-Coil Domain

Urs B. Hagemann, Jody M. Mason, Kristian M. Müller and Katja M. Arndt*

Institute for Biology III, Albert-Ludwigs-University of Freiburg, Schaenzlestrass 1, D-79104 Freiburg, Germany

Received 11 December 2007; received in revised form 7 April 2008; accepted 11 April 2008
Available online 17 May 2008

The activator protein-1 (AP-1) complex plays a crucial role in numerous pathways, and its ability to induce tumorigenesis is well documented. Thus, AP-1 represents an interesting therapeutic target. We selected peptides from phage display and compared their ability to disrupt the cFos/cJun interaction to a previously described *in vivo* protein-fragment complementation assay (PCA). A cJun-based library was screened to enrich for peptides that disrupt the AP-1 complex by binding to the cFos coiled-coil domain. Interestingly, phage display identified one helix, $JunW_{Ph1}$ [phage-selected winning peptide (clone 1) targeting cFos], which differs in only 2 out of 10 randomized positions to JunW (PCA-selected winning peptide targeting cFos). Phage-selected peptides revealed higher affinity to cFos than wild-type cJun, harboring a T_m of 53 °C compared to 16 °C for cFos/cJun or 44 °C for cFos/JunW. In PCA growth assays in the presence of cJun as competitor, phage-selected $JunW_{Ph1}$ conferred shorter generation times than JunW. Bacterial growth was barely detectable, using $JunW_{Ph1}$ as a competitor for the wild-type cJun/cFos interaction, indicating efficient cFos removal from the dimeric wild-type complex. Importantly, all inhibitory peptides were able to interfere with DNA binding as demonstrated in gel shift assays. The selected sequences have consequently improved our 'bZIP coiled-coil interaction prediction algorithm' in distinguishing interacting from noninteracting coiled-coil sequences. Predicting and manipulating protein interaction will accelerate the systems biology field, and generated peptides will be valuable tools for analytical and biomedical applications.

Keywords: AP-1; protein stability and specificity; leucine zipper; library selection; protein design and engineering

Edited by C. R. Matthews

**Corresponding author.* E-mail address: katja@biologie.uni-freiburg.de.

Present address: J. M. Mason, Department of Biological Sciences, University of Essex, Wivenhoe Park, Colchester, Essex CO4 3SQ, UK.

Abbreviations used: AP-1, activator protein-1; bCIPA, bZIP coiled-coil interaction prediction algorithm; BSA, bovine serum albumin; C, core pairing; CD, circular dichroism; DHFR, dihydrofolate reductase; EDTA, ethylenediaminetetraacetic acid; EMSA, electrophoretic mobility shift assay; ES, electrostatics; GST, glutathione *S*-transferase; HP, helix propensity; JunW, PCA-selected winning peptide targeting cFos; $JunW_{Phx}$, phage-selected winning peptide (clone *x*) targeting cFos; PCA, protein-fragment complementation assay; PEG, polyethylene glycol; PV hypothesis, peptide Velcro hypothesis; SEC, size-exclusion chromatography; TPA, 12-*O*-tetradecanoylphorbol-13-acetate; TRE, TPA-response element.

Introduction

The activator protein-1 (AP-1) transcription factor family, with chief constituents cJun and cFos, was first identified from viral homologues of its cellular oncogenic counterparts.[1,2] Its ability to induce tumorigenesis and its role in cancer are well documented. For example, it has been shown that cFos possesses the ability to induce osteosarcomas in mice,[3] whereas cJun is proposed to be more important in the development of skin and liver tumors.[4,5] AP-1 induction is mediated through several external stimuli that increase mitogen-activated protein kinase activity. The list of AP-1 target genes is large owing to the fact that AP-1 is a dimeric complex of members of the Jun, Fos, ATF, and Maf protein families. These interact with one another, generating a large set of possible interaction partners, and these different complexes determine the genes to be activated.[6] It is not surprising, therefore, that AP-1 plays key roles in cell proliferation, apoptosis, cell survival, and cell differentiation[7] and, thus, is an important target for therapeutic applications.

AP-1 members belong to the bZIP transcription factor family, which is characterized by a DNA binding 'basic' region and a coiled-coil (leucine zipper) domain. The coiled-coil domain is one of the most important protein–protein interaction motifs. Despite their abundance, their similarity in sequence, and their seemingly simple domain structure, coiled coils are highly specific, enabling them to form fine-tuned networks of homo- and heterotypic interactions. A set of different interhelical electrostatic interactions in the coiled-coil region provides stability and influences pairing preferences.[8–11] The periodicity of such a coiled coil is defined by a heptad repeat **[a–b–c–d–e–f–g]**$_n$. The core '**a**' and '**d**' positions are occupied by hydrophobic amino acids and are important for interhelical contacts, which contribute to the largest part of the interaction surface. The characteristic packing of the hydrophobic core was first described as 'knobs into holes' packing by Crick.[12] Typically, polar or charged amino acids occupy the **e** and **g** positions and aid in driving stability and specificity by increasing the solubility of the protein. Furthermore, these **e**/**g** edge positions can shield the hydrophobic core from aqueous surroundings.[13–15] Consequently, changing the amino acids in the interacting core and edge positions will either disrupt the interaction or lead to an interaction with improved stability relative to the wild-type interaction.

Coiled-coil interaction has been studied extensively, mostly by mutational analyses at selected singular sites or by rational design studies.[16–21] However, this work fails to encompass the diversity of sequence variations found in natural coiled-coil proteins. Most approaches use oversimplified sequences for the generation of coiled coils with specific properties,[14,15,22] often following the so-called peptide Velcro (PV) hypothesis,[23] an abbreviation in reference to one of the first successful designs of a heterodimeric coiled coil.[24] According to the PV hypothesis, complementary charged pairs on the edge of the interface (**e** and **g** positions) that relieve repulsive pairs in alternate oligomers are sufficient to promote formation of hetero-oligomers in natural and designed sequences.[9,11,24–27] While the PV hypothesis does not impose physical or structural details, this idea successfully predicts the pairing preferences of some[11,28,29] but not other[23,30–33] coiled coils. Furthermore, natural coiled coils (such as cFos) often deviate from the PV hypothesis; thus, targeting these sequences requires a different design strategy.

By inhibiting specific dimer formation, for example, cFos/cJun, it is possible to decrease target gene activation, which, in turn, can reduce oncogenic properties.[34] In fact, no mutations have been found in the cJun or cFos leucine zipper motifs. Rather, it is the higher abundance of these proteins (leading to increased DNA binding) that is concomitant with constitutively active pathways in human tumor cells.[35]

A previous study used the protein-fragment complementation assay (PCA) system[36] in which the murine enzyme dihydrofolate reductase (DHFR) is split into two halves. Library members and target sequence are each fused to one DHFR fragment and are coexpressed in *Escherichia coli*. Bacterial growth is restricted to interaction of the coiled-coil regions as they mediate the fully active state of the murine enzyme DHFR. This selection led to enrichment of a cFos-binding helix, JunW (PCA-selected winning peptide targeting cFos), from a library comprising 1.6×10^5 cJun variants.[37] The JunW/cFos complex displayed a T_m of 44 °C and a $K_{d,20\ °C}$ of 12 μM compared to wild-type cJun/cFos harboring an estimated T_m of 16 °C and a $K_{d,20\ °C}$ of 690 μM. By using such an inhibitory peptide, disruption of the wild-type interaction (and, hence, the onset of tumorigenesis) is a promising therapeutic goal.

In this study, we compared these results to phage display using identical libraries and targets. We sought to determine whether screening the same library with phage display would enrich for the same helix or for a helix with alternative residues and, hence, different properties. To our knowledge, this is the first direct comparison of these two selection systems. The main difference between both selection systems is that phage display expression occurs in the periplasm and selection is carried out *in vitro* under strictly controlled conditions, whereas PCA expression and selection occur *in vivo*, in the cytoplasm of the cell.

Using phage display, we enriched two helices, $JunW_{Ph1}$ and $JunW_{Ph2}$ [phage-selected winning peptides (clones 1 and 2, respectively) targeting cFos]. Both have a higher T_m in complex with cFos than the PCA-selected JunW and are able to successfully compete with cJun, which is concomitant with increased specificity towards cFos. Furthermore, all selected peptides form dimeric complexes as demonstrated by size-exclusion chromatography (SEC).

Finally, electrophoretic mobility shift assays (EMSAs) were performed, demonstrating the power of the improved leucine zipper stability. Importantly, all peptides were able to interfere with cFos/cJun dimerization also in the presence of its target DNA.

Results

In the present study, we generated peptides targeting cFos and compared two powerful selection systems, phage display and PCA. Resulting peptides were analyzed in terms of affinity, stability, and specificity. For direct comparison, we used a previously designed library of cJun variants that had been described in conjunction with the PCA system to select cFos-binding peptides.[37] Helix positions **a1**, **a2**, **a4**, and **a5** of the library retained wild-type residues and included a choice of T, V, I (β-branched), and A (Table 1; also see Ref. 37). Position **a3** was randomized to K, I, and wild-type N. The position **e3** was mutated from wild-type A to a choice of R, K, and Q as these charged or polar amino acids were predicted to make a favorable contact to **g2** E in cFos. All cJun **g** positions were retained in the library design, with additional options added to yield a set of potentially attractive interactions with cFos **e** positions. Excepting the **c1** position, which was changed to E to include a capping motif at the N-terminus, and **b3** Y for concentration determination, all remaining wild-type positions were retained. Previously, PCA screening of this library resulted in a winning peptide termed JunW with significantly improved binding affinity towards cFos compared to wild-type cJun/cFos interaction.[37] In the presented work, we compare this peptide to sequences selected with phage display.

Phage selection and analysis

Library-displaying phages were selected for binders against the coiled-coil domain of the target protein cFos. Selection was carried out at 37 °C to resemble physiological conditions and to be directly comparable to the previously performed PCA selection. To select only for the tightest interacting phages, we used trypsin in the elution process rather than acidic elution where complexes stable at low pH might be lost. After four selection rounds, sequencing of the whole library pool as well as of 10 individual clones showed that sequences had settled to a very similar set of amino acids. $JunW_{Ph1}$ was found in 2 out of 10 sequences (clones 1 and 8; see Table 1), and $JunW_{Ph2}$ was found in 3 sequences (clones 2, 6, and 9). Importantly, the sequence of the selected pool was very similar to the $JunW_{Ph1}$ sequence. Reassuringly, $JunW_{Ph1}$ differed only in positions **e3** ($JunW_{Q21R}$) and **g3** ($JunW_{E23K}$) from the JunW helix (Fig. 1).[45] The probability of these two contrasting selection systems arriving at such similar sequences by chance is unfeasibly low, indicating that both systems indeed selected for similar properties. The sequence of helix $JunW_{Ph2}$ differs from the sequences of $JunW_{Ph1}$ and JunW especially in the hydrophobic core. Valine was selected three times, at positions **a1**, **a2**, and **a5**, while A was selected at position **a1** and I at position **a5** in $JunW_{Ph1}$ and JunW. These positions pair in cFos with T at **a1** and **a2** and with K at **a5**. Position **a3**, opposing K in cFos, is occupied by I in all selected clones and was also manifested early during selection, indicating a clear preference over the other choices offered (K and N). Surprisingly, at position **a4**, R was found in $JunW_{Ph2}$ instead of one of the library amino acid options (T, I, V, or A), probably introduced by a point mutation. Possibly, R_{a4} interacts favorably with E at the cFos **g3** position, thereby also shielding the hydrophobic core from solvent (Fig. 1). In contrast to JunW, all phage-selected helices harbor basic amino acids at the **e3** position (R in $JunW_{Ph1}$ and K in $JunW_{Ph2}$), opposing E_{g2} in cFos. Positions **g2** and **g3** in $JunW_{Ph2}$ are identical with wild-type cJun.

Table 1. Amino acid sequences of cJun, Jun library, the phage pool, and enriched clones after four panning rounds

Clones	Amino acid sequence																			
cJun	AS		IARLEEK			VKTLKAQ			NYELAST			ANMLREQ			VAQL		GAP
	AS		IAELEEK			VKTLKAQ			NYELRST			ANMLREQ			VAQL		GAP
Jun-Library			T		Q	T		E	I		K A	T		H	T		
			V		R	I		K	K		Q K	I			I		
			A			A					E	V			A		
Interacting residue in cFos[a]			↓		↓	↓		↓	↓		↓ ↓	↓			↓		
			T		E	T		Q	K		E L	I			K		
Pool after panning round IV			A/V		R	V		E	I		R K/T	A		Q	I		
$JunW_{Ph1}$ (clones 1, 8)[b]			A		R	V		E	I		R K	A		Q	I		
$JunW_{Ph2}$ (clones 2, 6, 9)[c]			V		R	V		Q	I		K T	R		Q	V		
$JunW_{Ph3}$			V		R	A		Q	I		K T	A		Q	I		
$JunW_{Ph4}$			A		R	V		E	I		R T	A		Q	I		
$JunW_{Ph5}$			V		R	V		E	I		R T	A		Q	I		
$JunW_{Ph7}$			V		R	V		E	I		R K	A		H	I		
$JunW_{Ph10}$			V		R	A		E	I		K K	A		Q	I		
JunW[d]			A		R	V		E	I		Q E	A		Q	I		
Heptad repeat			abcdefg			abcdefg			abcdefg			abcdefg			abcd		

[a] For all library positions, the interacting partner of cFos is indicated, assuming the typical coiled coil pairs $a_i - a'_i$, $g_i - e'_{i+1}$ and $e_i - g'_{i-1}$ (where i denotes a given heptad and $i+1$ or $i-1$ denotes the following or preceding heptad, respectively).
[b] $JunW_{Ph1}$ has been found twice (clones 1 and 8).
[c] $JunW_{Ph2}$ has been found three times (clones 2, 6, and 9).
[d] PCA-selected JunW.[37]

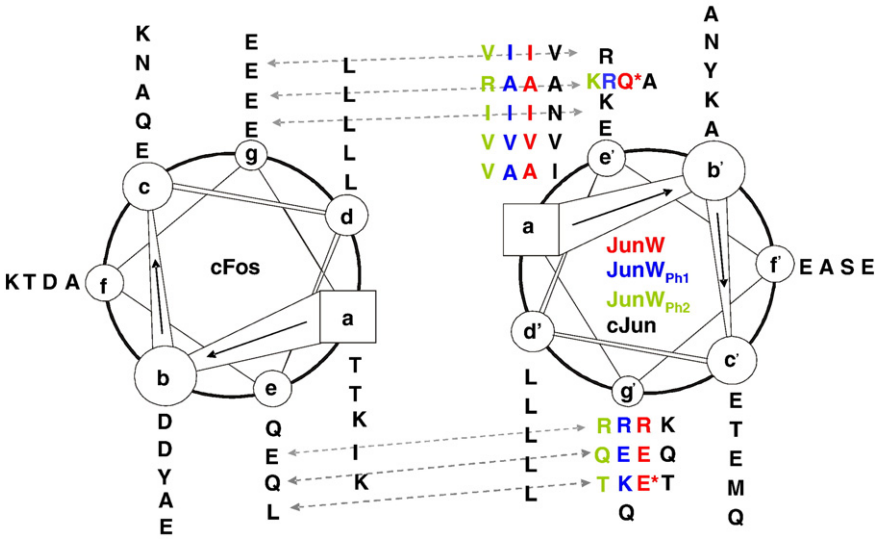

Fig. 1. Helical wheel representation of phage-selected helices JunW$_{Ph1}$ (blue) and JunW$_{Ph2}$ (green) in comparison to the PCA-selected JunW helix (red) and wild-type cJun (black). The two mutations of JunW with respect to JunW$_{Ph1}$ at positions **e3** (JunW$_{Q21R}$) and **g3** (JunW$_{E23K}$) are indicated by an asterisk. These intermediates, JunW$_{Q21R}$ and JunW$_{E23K}$, served to study epistasis of mutational space.

Binding affinities were analyzed by phage ELISA experiments with glutathione *S*-transferase (GST)–cFos as target (Fig. 2). We compared binding of phages displaying phage-selected clones, PCA-selected JunW, wild-type cJun, or a short mock peptide. As a control for specific binding, we also monitored binding to a GST surface. The ELISA revealed that all helices could be displayed and that binding was specific for GST–cFos (Fig. 2). Phage-selected helices JunW$_{Ph1}$, JunW$_{Ph2}$, and JunW$_{Ph4}$ showed significantly higher affinity and specificity to cFos than JunW. We chose JunW$_{Ph1}$ and JunW$_{Ph2}$ for further characterization as these displayed highest binding and the lowest unspecific signal. Furthermore, the difference of JunW$_{Ph1}$ and JunW$_{Ph4}$ was only one amino acid (K or T at **g3**), while JunW$_{Ph2}$ had six differences (including an additional R in the core) with respect to JunW$_{Ph1}$, making this sequence more interesting for further characterization. Also, comparing JunW$_{Ph1}$ and JunW$_{Ph2}$ to wild-type cJun, signals were about three to four times higher on GST–cFos surfaces and about three times lower on GST surfaces, indicating an impressive improvement in binding affinity. The low binding affinity of the cJun helix can be explained by the low stability of the cFos/cJun leucine zipper domain at 37 °C (see Table 4).

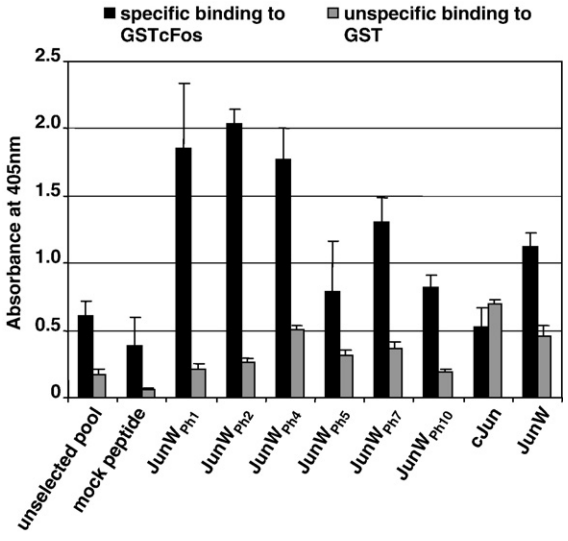

Fig. 2. Phage ELISA of various Jun-displaying phages on GST–cFos (black bars) or GST (gray bars) surface. Phage-selected helices as well as PCA-selected JunW and wild-type cJun were presented on phages and probed for binding in comparison to the unselected phage pool P0 using 10^{12} phages/well. A mock peptide displayed on phage served as control to demonstrate specific binding.

Protein-fragment complementation assay

The next step was to compare the performance of all peptides in the PCA system, which had led to the selection of JunW. In the PCA system, the bacterial survival is directly coupled to coiled-coil-mediated complementation of the DHFR fragments.[36] Cell growth was measured as an indicator of coiled-coil interaction. All phage- and PCA-selected helices conferred similar cell growth with doubling times of around 2 h, which was significantly faster than that for clones with wild-type cJun/cFos helices, which displayed a doubling time of more than 4 h (Table 2). Surprisingly, no significant differences were found between phage-selected and PCA-selected helices, which stands in contrast to phage ELISA data and denaturation experiments (see below) where JunW$_{Ph1}$ and JunW$_{Ph2}$ were found to bind cFos with higher affinity than JunW. A possible explanation could be a different expression level of the different helices in fusion with the DHFR fragment during PCA growth assay. Therefore, we analyzed helix-tagged DHFR fragments from cells grown under PCA conditions by SDS-PAGE and Western blotting (Fig.

Table 2. Calculated doubling times (in hours) of bacterial growths for different PCA settings

Samples[a]	Growth assay	Growth assay with cJun as competitor[b]	Growth assay with nonspecific peptide[b]	Growth assay with $JunW_{Ph1}$ as competitor[b]
cFos/JunW	2.06±0.02	8.28±0.08	4.48±0.02	–
cFos/$JunW_{Ph1}$	2.00±0.03	6.48±0.06	3.79±0.01	–
cFos/$JunW_{Ph2}$	2.05±0.02	6.54±0.11	–	–
cFos/cJun	4.42±0.50	14.12±0.45	5.43±0.17	17.23±0.88

[a] The first column indicates the sequences tagged to the DHFR fragments.
[b] The competitor (cJun or $JunW_{Ph1}$) or the mock peptide is expressed on a separate plasmid with a tetracycline resistance gene.

3). Interestingly, the Coomassie-stained gel (Fig. 3a) as well as the Western blot (Fig. 3b) showed a nearly three- to fourfold higher expression of DHFR-tagged JunW (band intensity increased by a factor of 3.6±0.4) compared to DHFR-tagged $JunW_{Ph1}$ and a twofold higher expression compared to DHFR-tagged $JunW_{Ph2}$ (2.2±0.2). This can be explained best by a mixture

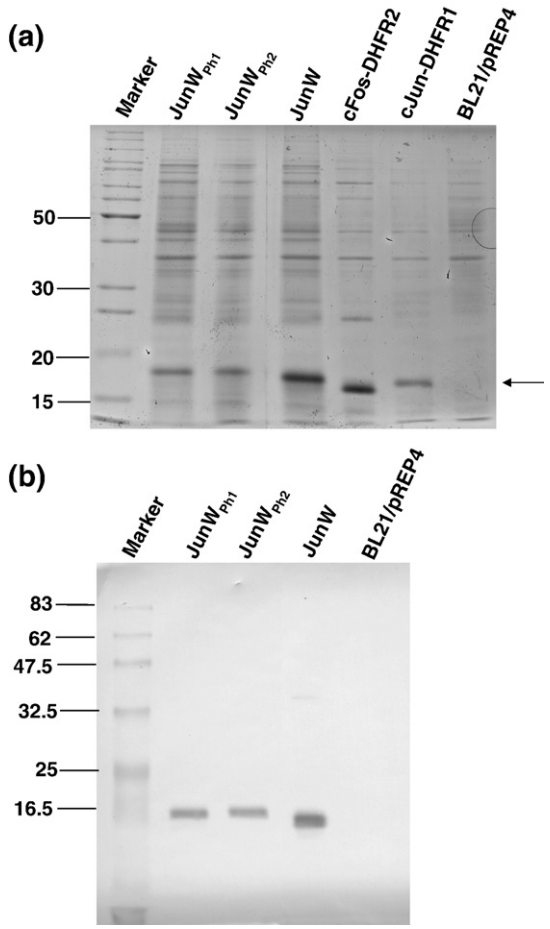

Fig. 3. SDS gel (a) and Western blot (b) analysis of PCA experiments with the various constructs. Ten microliters of an equivalence of $OD_{600}=2$ was loaded onto a 12.5% SDS polyacrylamide gel. (a) All JunW–DHFR1 fragments migrate at the expected size of ~18 kDa. Samples were normalized to the amount of cells before loading. About three to four times more JunW–DHFR1 is found compared to the phage-selected clones (arrow). cFos–DHFR2 (13.4 kDa) and cJun–DHFR1 are shown for comparison. BL21 cells transformed with pREP4 plasmid, but not with DHFR fragments, served as negative control. (b) Band intensity in the Western blot is consistent with the SDS gel.

of two effects: affinity differences can be compensated by expression levels and less proteolyic degradation and the possibility that the PCA cannot discriminate further once a certain threshold affinity is reached. While a threshold affinity is possible, it is unlikely have a significant influence as the PCA system also can select for higher affinities.[23]

A previous study in our laboratory used a competitive PCA selection to select for cFos interaction and, at the same time, disfavored interaction with cJun.[38] To include the same constraint in our assay and test the specificity of our phage-selected helices, we simultaneously expressed cJun in the abovementioned PCA. The cJun helix is not fused to any DHFR fragment, and therefore, any interaction should be inhibitory, preventing productive DHFR formation and, thus, resulting in severely impaired cell growth. Consequently, interaction and, hence, cell growth should depend not only on the binding affinity of the winner peptide to cFos but also on nonproductive binding to cJun. In addition, this provides a good comparison of JunW and $JunW_{Ph1}$. A summary of all doubling times from growth assays in the presence or absence of coexpressed cJun is listed in Table 2. As control, to account for stress imposed on the cell by the additional plasmid encoding cJun as well as a tetracycline resistance gene, we repeated experiments, expressing a short 6-aa-long mock peptide instead of cJun. As expected, growth was reduced due to additional antibiotic stress. However, this mock peptide did not affect growth to the same extent as cJun, and less variation was observed (Table 2). Consequently, observed growth differences are indeed due to cJun interfering with probe–target interaction. As expected, the slowest growth was observed in cells with wild-type cJun/cFos helices displaying a doubling time of more than 14 h. Cells expressing JunW/cFos displayed a generation time of 8.3 h compared to generation times of 6.5 h for $JunW_{Ph1}$/cFos and $JunW_{Ph2}$/cFos (Table 2). This effect can most likely be attributed to a lower specificity of JunW, which was confirmed by thermal denaturation experiments (see below and Table 4). Similarly, we tested cJun- and cFos-tagged DHFR fragments in the presence of $JunW_{Ph1}$, which seemed to be the most potent inhibitor (Table 2). Indeed, the doubling time of the cells expressing cJun/cFos was significantly impaired. The generation time dropped from 5.4 h (PCA in the presence of a mock peptide) to almost no detectable growth (17.2 h; PCA in the presence of $JunW_{Ph1}$), demonstrating the high inhibitory potential of this $JunW_{Ph1}$.

Analysis of oligomeric state

The helices were expressed as N-terminal fusion to GFP, spaced by a 16-aa-long linker, to assess the oligomeric state of the selected helices $JunW_{Ph1}$, $JunW_{Ph2}$, and JunW alone and in complex with cFos and cJun. Heteromeric and homomeric mixtures were loaded with a total concentration of 20 μM on a size-exclusion column. However, a run with 150 μM protein concentration gave a comparable result (see also Table 3). The mass of the eluting complexes was determined for all possible mixtures using a calibration curve, and the ratios between the obtained molecular weights and the theoretical monomeric weights were calculated (Table 3; Fig. 4). The mock control peptide fused to GFP eluted as a monomer (ratio $MW_{observed}$:$MW_{theoretical}$ = 1.1), demonstrating that GFP on its own does not induce dimerization. While we cannot rule out that there could be some steric hindrance from the GFP fusion, possibly disfavoring higher oligomers, we believe that this effect is minimal as we used a 16-aa-long flexible linker and also observed the formation of trimers with other peptide–GFP fusions (see Supplemental Fig. S1). The cFos/cJun mixture eluted in the range of a monomer (ratio of 1.3). This can be explained by the low stability of the cFos/cJun leucine zipper domain, harboring a K_d in the high micromolar range (see Table 4), thus representing equilibrium between monomer and dimer. The determined ratios for the mixtures cFos/$JunW_{Ph1}$, cFos/$JunW_{Ph2}$, and cFos/JunW are in excellent agreement with the calculated masses of dimeric complexes. We also injected mixtures of cJun in complex with the selected helices JunW, $JunW_{Ph1}$, and $JunW_{Ph2}$ (Fig. 4b). The mixture of cJun/JunW eluted as one peak, which indicates the formation of a stable complex. This is in agreement with thermal stabilities (see Table 4). In contrast, the mixtures cJun/$JunW_{Ph1}$ and cJun/$JunW_{Ph2}$ eluted as double peaks. These can be correlated to a cJun peak as well as to homodimeric complexes of the phage-selected helices when compared with Fig. 4c. These data demonstrate a weaker interaction between cJun and $JunW_{Ph1}$ and between cJun and $JunW_{Ph2}$, respectively, and are also in agreement with thermal denaturation experiments (Table 4). All homomeric mixtures of the selected peptides predominantly elute as dimers, and no higher oligomeric mixtures were observed. The low stability of cJun (estimated $K_{d,10\,°C}$ of 50 μM) explains why cJun homodimers elute in the range of a monomer rather than in the range of a dimer (Fig. 4c).

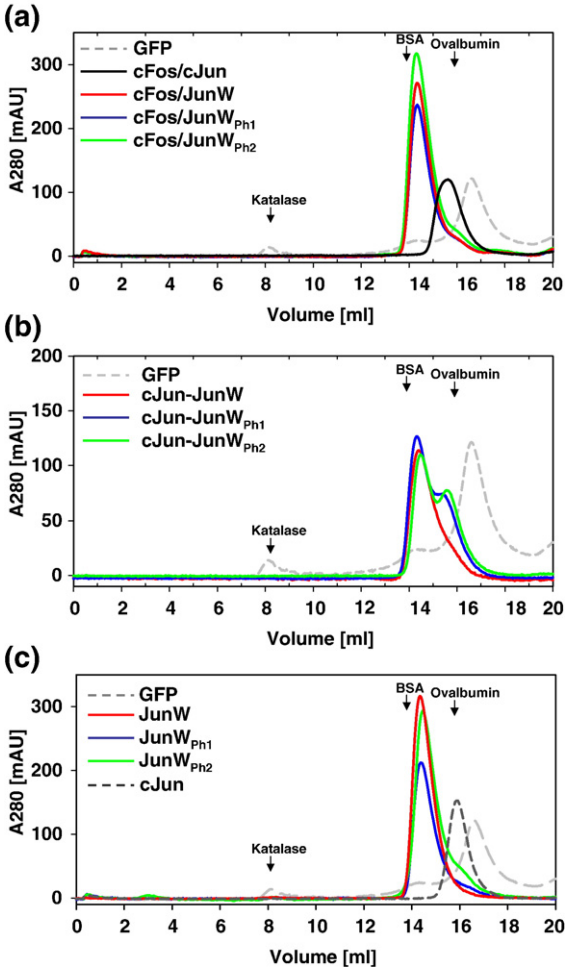

Fig. 4. SEC of all heterodimeric mixtures with cFos. The helices were loaded as N-terminal fusion to GFP at a concentration of 20 μM for each protein. Reassuringly, GFP does not influence the oligomerization state. The elution volumes of the calibration proteins catalase (232 kDa), BSA (67 kDa), and chicken ovalbumin (43 kDa) are indicated. (a) Heterodimeric mixtures with cFos. (b) Heterodimeric mixtures with cJun. (c) Homodimeric mixtures. Further controls are shown in Supplemental Fig. S1.

Table 3. SEC of GFP fusion proteins

GFP fusion proteins	Obtained MW (kDa)	Theoretical MW of monomers (kDa)	$MW_{obtained}$: $MW_{theoretical}$	Postulated complex
Mock	33.3	30.8	1.1	Monomer
cFos/cJun	44.3	32.9 + 32.9	1.3	Monomer
cFos/$JunW_{Ph1}$	63.5	32.9 + 32.9	1.94	Dimer
cFos/$JunW_{Ph2}$	64.4	32.9 + 32.9	1.95	Dimer
cFos/JunW	63.6	32.9 + 32.9	1.93	Dimer
cJun/cJun	40.7	32.9	1.2	Monomer
cJun/JunW	62.5	32.9 + 32.9	1.89	Dimer
cJun/$JunW_{Ph1}$	63.8 + 46.9	32.9 + 32.9	1.94 + 1.43	Dimer to monomer
cJun/$JunW_{Ph2}$	61.1 + 45.9	32.9 + 32.9	1.86 + 1.4	Dimer to monomer
JunW	63.5	32.9	1.93[a]	Dimer
$JunW_{Ph1}$	62.6	32.9	1.9	Dimer
$JunW_{Ph2}$	61.4	32.9	1.9	Dimer

[a] For comparison, JunW SEC runs were also performed at 150 μM and resulted in a $MW_{obtained}$:$MW_{theoretical}$ of 2.1.

In vitro stability of selected helices

Helices were characterized biophysically for stability and specificity alone as well as in complex with cFos and cJun. As $JunW_{Ph1}$ differs only in **e3** and **g3** from JunW, we analyzed these two positions in more detail by looking at the respective two single

Table 4. Summary of thermodynamic data derived from CD spectra and thermal denaturation experiments

Complex	T_m (°C)	ΔT_m (°C)[a]	$K_{d,20\ °C}$ (μM)[b]	ΔG (kcal/mol)	Ratio $[\Theta]_{222/208}$
cFos/cJun	16[c]	4.5	692	4.1	0.78
cFos/JunW$_{Ph1}$	53	27.5	2	7.7	1.01
cFos/JunW$_{Ph2}$	49	28.0	3	7.4	1.02
cFos/JunW	44[c]	11.5	12	6.6	1.04
cFos/JunW$_{Q21R}$	46	21.4	4.4	7.2	1.02
cFos/JunW$_{E23K}$	36 and 50[d]	n.d.	n.d.	n.d.	1.03
cJun/JunW$_{Ph1}$	(37)[e]	−1.0	(48)	(5.8)	0.83
cJun/JunW$_{Ph2}$	36	2.5	52	5.7	0.87
cJun/JunW	(57)[c]	12.0	(0.07)	(9.6)	0.96
JunW$_{Ph1}$	52		2.7	7.5	0.99
JunW$_{Ph2}$	43		11.3	6.6	1
JunW	66[c]		0.015	10.5	1.05
JunW$_{E23K}$	70		0.0081	10.8	1.03
JunW$_{Q21R}$	50		3.31	7.3	0.99

[a] The ΔT_m is the averaged T_m of the homodimers subtracted from the T_m of the heterodimer.
[b] Temperature-derived K_d values have been corrected according to Eq. (2).
[c] These values have been published.[37]
[d] The two transitions were estimated using the first derivative. Accordingly, no reliable K_d or ΔG values could be obtained.
[e] Values in parentheses are estimates as data were difficult to fit due to a very steep lower baseline.

mutants, JunW$_{Q21R}$ (facing E_{g2} in cFos) and JunW$_{E23K}$ (facing L_{e4} in cFos) (Fig. 1). Circular dichroism (CD) spectra were recorded at 5 °C for all possible heterodimeric combinations with cFos and cJun (data not shown). A ratio of $[\Theta]_{222/208}$ greater than 1.0 is a measure of interacting α-helices in benign media[39,40] (Table 4). All of the examined peptide mixtures, except wild-type cFos/cJun, revealed a ratio ≥1 in complex with cFos. This indicates the formation of a well-folded coiled coil. Interestingly, complexes with cJun showed ratios <1, which indicates a poorly folded coiled coil.

Thermal denaturation was performed to monitor protein unfolding. A plot of all measured heterodimers and homodimers is shown in Fig. 5, and a summary of T_m values as well as estimated K_d and ΔG values is given in Table 4. All complexes exhibited a cooperative two-state unfolding, except cFos/JunW$_{E23K}$, which showed two transitions. Interestingly, adding the Q21R mutation to the JunW$_{E23K}$ variant (JunW$_{Q21R,\ E23K}$ identical with JunW$_{Ph1}$) again showed a two-state transition. While the wild-type cJun/cFos coiled-coil interaction has a T_m of only 16 °C and an estimated $K_{d,20\ °C}$ in the upper micromolar range, all other complexes were significantly more stable. This seemingly low stability of cJun/cFos is explained by the fact that we used only the leucine zipper domain in our analysis. The wild-type protein gets significantly stabilized by DNA binding.[34] Furthermore, other groups often used disulfide-bridged peptides or longer versions, including the basic regions,[41] to determine the stability of the Jun–Fos complex. A detailed comparison of the stabilities of cJun/cFos with data in the literature is provided in Mason *et al.*[37]

The complex cFos/JunW$_{Ph1}$ displayed a T_m of 53 °C with an estimated $K_{d,20\ °C}$ of 2 μM compared to the complex cFos/JunW$_{Ph2}$ harboring a T_m of 49 °C and an estimated $K_{d,20\ °C}$ of 3 μM and cFos/JunW with a T_m of 44 °C and an estimated $K_{d,20\ °C}$ of 12 μM. Thus, compared to cJun, all selected helices have

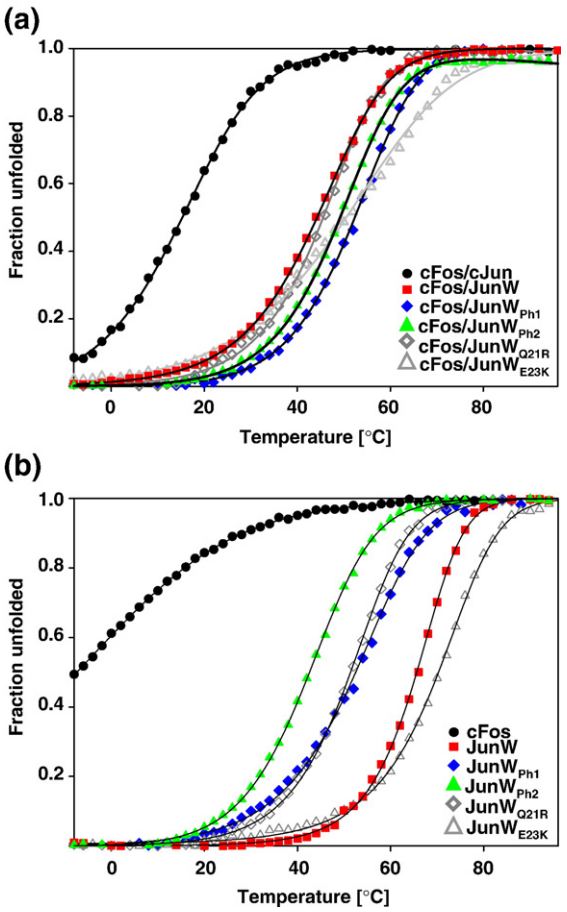

Fig. 5. Temperature-induced denaturation followed by $CD_{222\ nm}$ of (a) heterotypic and (b) homotypic complexes (150 μM total peptide concentration). Symbols represent measured data, and continuous lines denote the respective fits assuming a two-state transition. All fits agree well with measured data except cFos/JunW$_{E23K}$, which displays partial three-state characteristics at this concentration.

significantly improved affinity towards cFos, being 37 °C, 33 °C, and 28 °C more stable than the wild-type cFos/cJun interaction. Compared to JunW, the mutant $JunW_{Q21R}$ has a slightly increased T_m of 46 °C in complex with cFos. The mutant $JunW_{E23K}$ displays a three-state behavior with two transitions estimated to occur around 36 °C and 50 °C.

Additionally, $JunW_{Ph1}$ and $JunW_{Ph2}$ have higher specificity than JunW in binding cFos over cJun (Table 4; Fig. 5). In comparison to JunW, which harbors a T_m of 57 °C in complex with cJun, both phage-selected helices show a significant decrease in cJun affinity, although some of these data were difficult to fit due to steep lower baselines. We estimated a T_m of 37 °C and 36 °C for $JunW_{Ph1}$/cJun and $JunW_{Ph2}$/cJun complexes, respectively.

A stable heterotypic interaction is also seen by a more stable melting curve of the heterodimer compared to the averaged melting curves of the respective homodimers, which results in a positive ΔT_m when subtracting the averaged T_m values of the homodimers from the T_m of the heterodimer (see Supplemental Fig. S2). All JunW variants as well as cJun, albeit to a lower extent, give a large and positive ΔT_m value when paired with cFos, indicative of preferred heterodimer formation (Table 4). In contrast, ΔT_m values for cJun/JunW complexes are of similar value only for PCA-selected JunW but close to zero for the phage-selected $JunW_{Ph1}$ and $JunW_{Ph2}$, indicating no preference for cJun binding over homodimerization, consistent with the results from SEC experiments (Fig. 4). The homodimeric mixtures of the selected peptides all display a cooperative two-state transition curve, with the intermediate $JunW_{E23K}$ being the most stable (T_m of 70.3 °C). Phage-selected homodimers ($JunW_{Ph1}$ and $JunW_{Ph2}$) are less stable than the corresponding heterodimer with cFos, whereas DHFR-selected JunW and the intermediates form more stable homodimers.

Disruption of Jun–Fos heterodimers in EMSAs

Target gene activation of cJun/cFos heterodimers occurs via binding to the 12-*O*-tetradecanoylphorbol-13-acetate (TPA)-response element (TRE). The dimerization of cFos/cJun is driven by the leucine zipper domain, whereas the DNA binding occurs via the basic region N-terminal of the leucine zipper. This DNA binding significantly stabilizes the complex.[34] EMSAs were performed to investigate whether the selected inhibitors were capable of interfering not only with dimerization but also with DNA binding. GFP-tagged target proteins, including their basic DNA-binding regions (basic-cJun/basic-cFos), were mixed as heterodimers and in combination with a 2-fold and 20-fold molar excess of cJun, $JunW_{Ph1}$, $JunW_{Ph2}$, or JunW and incubated with the DNA containing the AP-1 recognition sequence, the TRE (Fig. 7). All selected peptides interfered with DNA binding already at a 2-fold molar excess of competitor. The DNA binding is almost completely abolished at a 20-fold excess of competitors. In contrast, cJun demonstrated none or only very weak interference with the DNA binding. Importantly, a similar result is obtained when the peptide inhibitors are added to the preformed cFos:cJun:DNA complex (Fig. 7b), demonstrating the ability of the selected peptides to efficiently abolish DNA binding. To test the specificity of the selected peptides, we performed a second gel shift assay (Fig. 7c). The peptides were mixed together with the bHLHZip domains of the human transcription factors Myc/Max in the presence of its DNA recognition sequence (E-box DNA). No reduction of the signal was observed even at a 20-fold molar excess of competitor. This result demonstrates that the selected peptides solely target the cFos–leucine zipper domain, manifesting our design and selection strategy. The controls shown in Fig. 7d demonstrate that the wild-type mixture basic-cFos/basic-cJun exclusively binds the TRE DNA and not the E-box control DNA. In addition, GFP does not bind the TRE DNA.

Correlation of stabilities with sequence properties

As mutations in coiled coils often act independent from each other, ΔG values of the various complexes (Table 4) were correlated with their respective sequences (Table 1). The mutation Q21R in **e3**, opposing E_{g2} in cFos, is predicted to improve electrostatic interactions. Indeed, the estimated energy difference from the measured stabilities between cFos/$JunW_{Q21R}$ and cFos/JunW, $\Delta\Delta G$ of −0.6 kcal/mol (Table 4), is in excellent agreement with data from Krylov *et al.*,[19] who published an energy difference for an $E_gQ_e \rightarrow E_gR_e$ exchange of −0.6 kcal/mol (Fig. 6) albeit in a different coiled-coil context. Introducing the second mutation, E23K (opposing L_{e4} in cFos), in the $JunW_{Q21R}$ peptide results in the peptide

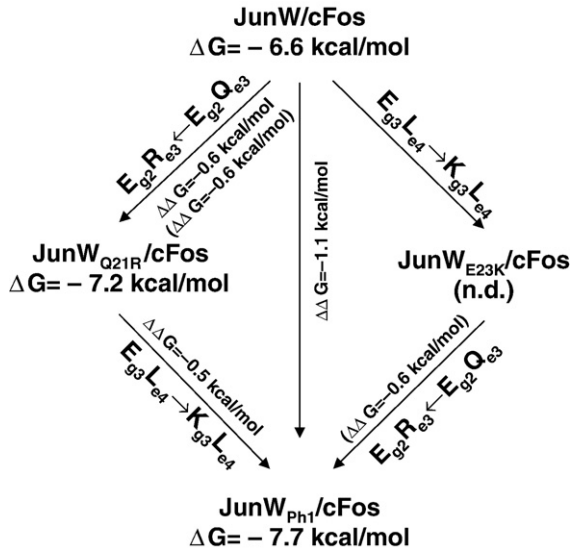

Fig. 6. Mutant cycle of JunW, $JunW_{Q21R}$, $JunW_{E23K}$, and $JunW_{Ph1}$ in complex with cFos. Measured ΔG values are indicated for each complex. Changes of **g**/**e** pairs are shown as well as calculated $\Delta\Delta G$ values. $\Delta\Delta G$ values from literature are enclosed in parentheses.

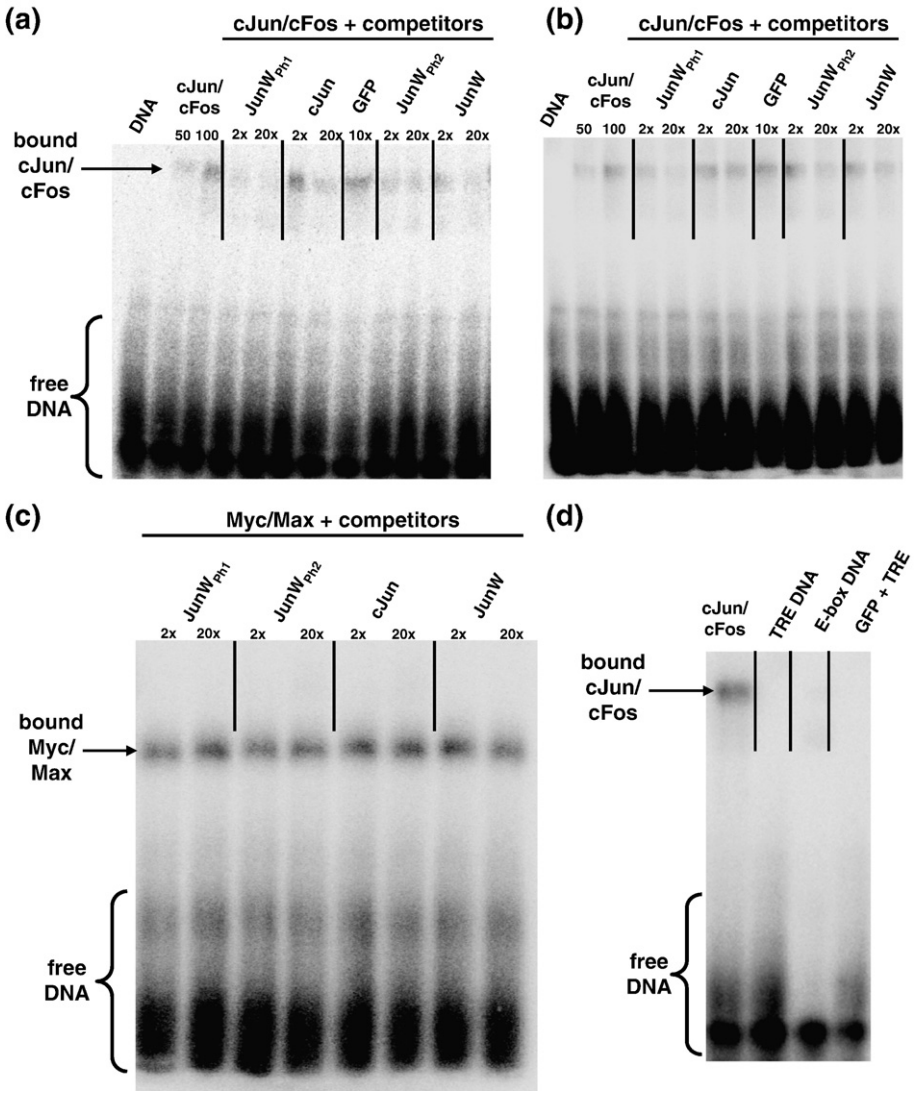

Fig. 7. EMSA analysis of the DNA-bound Jun–Fos in the absence or presence of peptides JunW$_{Ph1}$, JunW$_{Ph2}$, JunW, and cJun as competitors. (a and b) bZIP domains of Jun and Fos were expressed as N-terminal fusions to GFP and used at a concentration of 100 ng each except for lane 1 (DNA only) and lane 2 (50 ng each). Lanes 4–12, Jun, Fos, and DNA were incubated with 2-fold and 20-fold excess of indicated inhibitors (a) directly or (b) after 15 min preincubation of the Jun:Fos: DNA complex. (c) Twofold and 20-fold excess of peptide was incubated in the mixture with the control proteins basic-Myc and basic-Max (bHLHZip domain) in the presence of Myc/Max DNA (E-box DNA) to assess the specificity of the selected peptides. (d) Negative controls to prove that neither basic-cJun/basic-cFos bound to the control E-box DNA (lane 3) nor GFP bound to the TRE DNA (lane 4).

JunW$_{Ph1}$. We measured a difference in energy of −0.5 kcal/mol for the $E_{g3}L_{e4} \rightarrow K_{g3}L_{e4}$ change. No published data are available for comparison. Due to the three-state transition of the JunW$_{E23K}$/cFos complex, the alternative way JunW → JunW$_{E23K}$ → JunW$_{Ph1}$ (right leg in Fig. 6) could not be calculated. However, the measured $\Delta\Delta G$ change for the double mutation leading from JunW to JunW$_{Ph1}$ ($\Delta\Delta G$ of −1.1 kcal/mol) represents the sum of both single mutations. This confirms the additive behavior.

Prediction of coiled-coil interaction is very desirable because of the importance of this motif and the regularity of the structure. Data obtained from this study as well as data from other sources[18–21,23,38] were used to improve our previously developed algorithm bCIPA (bZIP coiled-coil interaction prediction algorithm†[37]). This algorithm uses simple scoring matrices for **a**/**a** and **d**/**d** core pairing (C), **g**/**e** electrostatics (ES), and helix propensity (HP) to predict T_m data. By adjusting matrices and fitting parameters with the new data, we obtained good agreement between calculated and measured T_m values ($\chi^2 = 0.76$). Furthermore, using this algorithm for the prediction of an independent data set of bZIP coiled coils,[41] we were able to increase the percentage of correctly predicted strong interactions from 92% to 97% and the percentage from correctly

† www.molbiotech.uni-freiburg.de/bCIPA

predicted noninteraction from 92% to 95%. The new algorithm will be available on our web site†.

Discussion

The transcription factor AP-1 plays a key role in numerous pathways that are often found to be deregulated in tumors. Consequently, peptides targeting AP-1 components and thereby modulating their function will be powerful tools to dissect pathways and will identify novel strategies for the design of therapeutics. The generation of such tailored molecules requires an efficient design and/or selection strategy.[42] Phage display is one of the most commonly used methods for rapid selection of proteins binding to a target of interest.

Another phage display study had been reported using the heterodimer Acid-p1/Base-p1 as scaffold.[43] In that study, Base-p1 was destabilized by mutating the **a4** position from L to A. Neighboring residues in Acid-p1 (**d3**, **g3**, **a4**, and **d4**) were randomized, and selection against mutated Base-p1 resulted in enrichment of the residues L (**d3**), E (**g3**), I (**a4**), and M (**d4**) and a significantly improved stability. Comparable to those results, where the destabilizing A was compensated by an I at the opposing **a**′ position, in all selected clones (excepting $JunW_{Ph2}$ where an additional mutation occurred; see Table 1), wild-type A_{a4} was retained opposing $I_{a'4}$ in cFos. Similarly, a previous screening of a library directed against cJun selected I over other hydrophobic options at that library position pairing with A_{a4} in cJun.[37]

Here, we compared phage display with another highly successful selection system, the split-DHFR PCA. While both systems express proteins in *E. coli*, they have fundamental differences: Phage display requires proteins to locate and fold in the periplasm, and selection occurs *in vitro* under artificial conditions. In contrast, in PCA, expression and selection occur in the cytoplasm of *E. coli* in the presence of a vast number of cellular proteins. To test in what respect these factors influence selection, we compared phage display selection of a semirandomized library directed against the coiled-coil domain of the oncoprotein cFos with previously reported results from PCA selection[37] using the same library. Reassuringly, phage-selected clones were very similar, albeit not identical, to PCA-selected JunW, indicating that binding properties clearly dominated the selection.

All selected clones showed significantly increased binding affinity towards cFos with T_m values between 44 °C and 53 °C compared to 16 °C for the wild-type cJun/cFos coiled-coil complex. The peptides displayed a two-state unfolding with the exception of cFos/$JunW_{E23K}$, which gave rise to two transitions. Such a switch between two- and three-state unfolding pathway caused by only minor changes in sequence has been reported earlier.[44] Recently, we investigated the kinetics of complex formation between cFos and JunW, $JunW_{Ph1}$, and the intermediate mutants ($JunW_{Q21R}$, $JunW_{E23K}$) using stopped-flow analysis.[45] This study revealed that all of the possible peptide mixtures fold via a transiently populated dimeric intermediate. Of these, cFos–$JunW_{E23K}$ is the only dimer where the intermediate can be detected by equilibrium denaturation. SEC experiments confirmed that all selected peptides form dimeric complexes in mixture with cFos. From these peptides, JunW is the only one that exhibits tight binding also towards cJun as determined by thermal denaturation (ΔT_m values) and also seen by SEC experiments.

The ranking of stabilities from phage ELISA signals fits with the measured T_m values from thermal melts, where $JunW_{Ph1}$ and $JunW_{Ph2}$ showed higher affinities than JunW towards cFos. Some differences were observed in the PCA system, where clones $JunW_{Ph1}$, $JunW_{Ph2}$, and JunW performed about equally well. This apparent discrepancy can be explained by differences in expression level and/or proteolytic stability (Fig. 3), resulting in differences in the protein concentration during selection. Furthermore, a saturation of selection stringency in the PCA system cannot be ruled out.

When expressing the cJun peptide as additional constraint in the PCA system, $JunW_{Ph1}$ performed better than JunW, which can be explained by the lower tendency of $JunW_{Ph1}$ to form homotypic interactions as well as complexes with cJun. Furthermore, adding the best competitor peptide, $JunW_{Ph1}$, in the PCA setting with wild-type cJun and cFos almost completely prevented growth, indicating nearly complete inhibition of wild-type complex formation. So far, most *in vivo* selections have used positive design strategies to maximize the stability of the desired structure. This extended PCA growth assay can be used for selecting helices in the presence of competing sequences, thereby including negative and competitive design.[38]

Important for the use of these inhibitors in cellular systems is the ability of the inhibitors to interfere not only with protein–protein interaction but also with DNA binding. Thus, we tested the potency of our selected peptides in EMSA. We demonstrated that the wild-type interaction in the presence of DNA is considerably impaired already at a twofold molar excess of the selected peptides. Importantly, the leucine zipper drives the interaction and also determines which interaction pair is being formed in the cellular network. In contrast to our approach, the designed acidic extension from Krylov *et al.* was fused to the wild-type leucine zipper domain of the transcription factors C/EBP,[46] Myc/Max,[47] or AP-1.[34] The inhibitory effect lies within the binding of the acidic extension, mimicking the charge of the DNA, with the basic domain of the cellular transcription factor. Hence, the dimerization of the transcription factor is prevented, which results in an inhibition of target gene activation. Thus, our designed and selected peptides alone or, even better, in combination with the acidic extension from Krylov *et al.* should therefore be of great interest for future cellular experiments and *in vivo* studies.

The PV hypothesis, while working well for most artificial sequences, fails to accurately predict several coiled-coil interactions. This is due to the extended sequence repertoire used in natural coiled coils *versus* designed ones that often are restricted to L at core **d** and to V, I, and N at core **a** positions as well as K, R, E, and Q residues at edge **e** and **g** positions for parallel dimeric coiled coils. Notably, the cFos coiled-coil sequence (which harbors two polar T and two charged K residues at four out of five **a** positions as well as an L at position **e4**) deviates from idealized coiled-coil sequences, thus complicating the design or prediction of tight binding partners. Consequently, our selected peptides with very similar but distinct sequences provide an excellent set to further our understanding about sequence requirements and pairing preferences. L_{e4} in cFos is predicted to pair with T, K, or E at **g3** of selected JunW peptides. None of these pairs is commonly found, and little is known about their contribution to overall stability and binding affinity. We measured a destabilization by approximately 0.5 kcal/mol for $E_{g3}L_{e4}$ (JunW/cFos) with respect to $K_{g3}L_{e4}$ ($JunW_{Ph1}$/cFos). Perhaps the longer side chain of K (four alkyl groups compared to two alkyl groups in E) can better shield the hydrophobic core from the aqueous solvent, and the hydrophobic character can be beneficial in the interaction with L_{e4} in cFos. In addition, K_{g3} could make beneficial intrahelical contacts with E_{c3}.

Deviations from typical core interactions hamper precise prediction further. Recently, a larger data set of possible core interactions became available.[20] While these data provide valuable insight in interaction preferences at coiled coil **a** positions, tabulated energies of reciprocal pairs differ by up to 1.3 kcal/mol, indicating a positional influence for some pairs. K in the core has been predicted to pair preferentially with I, and this is indeed what we observed at the core **a3** and **a5** positions, with only one exception, $JunW_{Ph2}$/cFos, where a $K_{a5}V_{a5}$ pair is found instead. cFos T_{a2} pairs preferentially with V, with exceptions $JunW_{Ph3}$/cFos and $JunW_{Ph10}$/cFos, where a $T_{a2}A_{a2}$ pair is found instead. This is also in accordance with published data, where TV and TI pairs are the most stable of all options investigated.[20] The pairing preference of cFos **a1** position is more difficult to rationalize. We observed examples of $T_{a1}A_{a1}$ and $T_{a1}V_{a1}$ pairs, and sequencing of the phage pool after four rounds showed for this position an about equal distribution between V and A, whereas all other randomized positions were clearly settled. Interestingly, a comparison of peptides suggested that $T_{a1}A_{a1}$ pairs were considerably more stable than $T_{a1}V_{a1}$ pairs, which is in contrast to observed pairing preferences of the **a2** position and to published values.[20] However, our observations agree with previous reports that show that sequence preferences at this particular position differ from those of the other core positions. In a mutational study, two (positions **a2** and **a4**), four (positions **a2**–**a5**), or all five cFos **a** positions were changed to I, and binding to cJun was probed.[48] Curiously, the peptide with wild-type **a1** T and only four core I residues (and even the peptide with only two core I residues) was superior to the version with five core I residues, although the latter had an $I_{a1}I_{a1}$ pair, predicted to be considerably more stable ($\Delta\Delta G \sim -7.5$ kcal/mol[20]) than the wild-type $T_{a1}I_{a1}$ pair.

In the "omics" era, a wealth of information about genes and proteins is available, but scientists still struggle to fit all pieces together to obtain a valid picture of an entire system. Consequently, a simple and fast yet reliable prediction of protein–protein interaction is desirable. In the light of the importance of the coiled-coil motif for protein–protein interaction, prediction of pairing preferences will have a great impact on systems biology. Despite all obstacles imposed by sequence irregularities, prediction of coiled-coil interaction is facilitated by the amount and quality of data available, especially for the overall more regular leucine zipper found in bZIP transcription factors. Including all Jun- and Fos-based variants described in this work, we improved performance of the bCIPA program[37] and are now able to correctly predict 97% of all strong interactions and 95% of all noninteracting pairs of an independent data set of human bZIP proteins.[41] This prediction is on par with a previously published prediction program[49] but uses very simple and easily adaptable scoring matrices.

The presented study not only permitted insight into features promoting coiled-coil stability and specificity but also generated a valuable set of AP-1-directed peptides that will be useful in downregulating AP-1 activity in tumor cells and, thus, have the potential to serve as lead compounds in innovative drug design. In addition, following this route, peptides directed against other proteins of interest can easily be generated and applied to manipulate protein function *in vivo*. These data paired with a reliable prediction program will aid in deciphering cellular networks.

Materials and Methods

Construction of the Jun library

The construction of the Jun library (see also Table 1 for randomized positions) has been described.[37] Briefly, overlapping oligonucleotides including relevant degenerate codons for desired residue options were designed, and overlap extension PCR was performed to generate a 111-bp oligonucleotide flanked by NheI and AscI restriction sites.

The M13KE vector (NEB) was modified by inserting a short NheI/AscI (underlined)-containing oligonucleotide (5′-ATCGCTGGTACCTTTCTATTCTCACTCGGCTA-GCGTGGAATTCTAACCACGATGGCGCGCCTGGCC-GAGGTGGCTGGCCGAACAGC-3′), which was cloned via Acc65I and EagI sites. This insert also encodes a Gly-Arg-Gly linker designed for a tryptic digest. The resulting phage vector was named M13KE–NheI–AscI. The library insert[37] was cloned into M13KE–NheI–AscI and transformed into XL-1 blue cells (Stratagene), resulting in the vector M13KE–Jun library. The library size of 140,000 was determined from phage titer in dilution series on top-agar IPTG (1 mM)/Xgal (5-Bromo-4-chloro-3-indolyl-β-D-galactoside) (1 mM) LB plates. The library pool was propagated in an LB or 2YT culture (25 μg/ml tetracycline) of ER2738 cells (NEB) for 4–6 h to amplify the phages.

Randomization was verified by sequencing, and an approximately equal distribution of the varied amino acids, except H at **g4**, was found. The genes for cJun and JunW[37] were cloned in the same manner into M13KE–NheI–AscI and transformed into XL-1 cells to yield M13KE–cJun or M13KE–JunW, respectively.

Target preparation

The gene for the target cFos, used for all panning rounds and ELISA experiments, was cloned as C-terminal fusions to GST. The GST gene was amplified out of pGEX-2T (GE Healthcare), which was a kind gift from Dr. G. Schmidt (Pharmacology, Freiburg, Germany), and cloned into pAR200d–DHFR2, a derivative of pQE16 (Qiagen). The forward primer contained a BseRI site (5′-GCAGTCGAGGAGAAATTAAGCATGTCCCCTATAC-TAGGT-3′), while the reverse primer contained the recognition site for the protease factor Xa (Ile-Glu-Gly-Arg) and an NheI site (5′-GCGCATGCTAGCACGACCTTC-GATCAGATCCGATTTTGGAGGA-3′). DHFR2 was removed by BssHII digestion and subsequent ligation resulting in the plasmid pAR200–GST. The gene for cFos was cloned into pAR200–GST using NheI and AscI sites, yielding pAR200–GST–cFos.

Target purification

The plasmid encoding the GST fusion protein (pAR200–GST–cFos) was transformed into RV308 cells together with the Lac repressor expressing plasmid pREP4 (Qiagen). A preculture was grown at 26 °C overnight in 2YT medium (100 μg/ml ampicillin and 50 μg/ml kanamycin). The preculture was diluted to an OD_{600} of 0.1 and induced (1 mM IPTG) at an OD_{600} of 0.5–0.6. Cells were harvested after 6 h and resuspended in lysis buffer (140 mM NaCl, 2.7 mM KCl, 10 mM Na_2HPO_4, and 1.8 mM KH_2PO_4, pH 7.3). Cells were lysed by sonication on ice for 10 min with 1-min interruption in between, and cell debris was spun down at 19,000*g* at 4 °C for 30 min. The supernatant was immediately loaded onto a GST affinity column (GSTrap HP, 1 ml; GE Healthcare), washed with 60 ml lysis buffer, and eluted with 10 mM reduced glutathione in 50 mM Tris, pH 8. Protein concentration was determined from absorbance spectra measurements at 280 nm after extensive dialysis against TBS (50 mM Tris/HCl and 150 mM NaCl, pH 7.5).

Phage purification and selection

Amplified phages from ER2738 cultures were centrifuged for 20 min at 4 °C and 5000*g* (Heraeus Varifuge). Phages were precipitated by addition of 1/6 vol of polyethylene glycol (PEG)/NaCl [20% (w/v) PEG 6000, 2.5 M NaCl] to the supernatant, incubation at 4 °C overnight, and centrifugation for 15 min at 4 °C and 5000*g* (Heraeus Varifuge). The phage pellet was resuspended in 1 ml of cold TBS and centrifuged for 5 min at 4 °C and 16,000*g* using a benchtop centrifuge. The supernatant was transferred into a fresh reaction tube for a second PEG/NaCl precipitation (incubation 1 h on ice and centrifugation for 8 min at 4 °C at 16,000*g*). The pellet was resuspended in 1 ml cold TBS. The phage concentration was determined spectroscopically according to:[50]

$$\text{phages/ml} = \frac{(A_{269} - A_{320}) \times 6 \times 10^{16}}{\text{phage genome in nt}} \times f, \qquad (1)$$

where the size of the phage genome is 7348 nt for the Jun library and 7271 nt for the mock peptide phage and f is the dilution factor.

Phage selection was carried out in 96-well microtiter plates (Maxisorb, Nunc). One hundred microliters of the purified, GST-tagged target protein cFos (30 μg/ml) was coated overnight at 4 °C and mild shaking. After washing four times with TBS, the surface was blocked with 350 μl bovine serum albumin (BSA) solution [3.5% (w/v)] for 2 h at 16 °C, washed four times with TBS, and coated again with 100 μl GST–cFos (30 μg/ml) for 1 h at 16 °C. All selection rounds were carried out at 37 °C with a phage titer of about 3×10^{12} pfu. Library-displaying phages were incubated on the target for 1 h at 37 °C. The number of washing steps with TBS containing 0.1% Tween was increased for each subsequent panning round (five times in panning round PI, 20 times in PII, 50 times in PIII, and 10 min under running tap water in PIV). Remaining phages were eluted using 100 μl trypsin solution (3 μg/ml in TBS and 1 mM $CaCl_2$, pH 7.5) for 20 min at 37 °C. ER2738 *E. coli* cultures were grown in LB medium (25 μg/ml tetracycline) and subsequently at an OD_{600} of 0.3–0.5 infected with eluted phages and grown for 4–6 h at 37 °C for phage amplification. After panning round IV, 10 individual clones were sequenced (Table 1).

Phage ELISA experiments

Ninety-six-well plates were coated and blocked identically to the procedure used for phage selection. Phages ($1–2 \times 10^{12}$ pfu) were incubated at 37 °C for 1 h on the target GST–cFos. Unbound phages as well as nonspecific phages were removed by washing 20–30 times with TBS, 0.1% Tween. Bound phages were detected by incubating with an anti-M13KE antibody coupled to horseradish peroxidase (GE Healthcare) for 1 h at 20 °C using a dilution of 1:1000 (TBS, 0.3% BSA). Antibody solution was removed by washing 3 times with TBS, and detection was performed with 2,2′-azino-di-[3-ethylbenzthiazolin-sulfonat(6)] solution (Roche, 100 μl, 1 mg/ml).

Construction of DHFR fragments and growth assay

Double-stranded phage DNA inserts for selected helices were digested with NheI and AscI, gel purified, and ligated into the vector pAR200–DHFR1 (described elsewhere[37]), yielding the plasmids pAR200–$JunW_{Ph1}$–DHFR1 and pAR200–$JunW_{Ph2}$–DHFR1. For the competition PCA, the genes for the competitor cJun or $JunW_{Ph1}$ as well as for a mock peptide (ASWNSNHDGAP) were cloned via NheI and AscI into the vector pAR410 (tetracycline resistance[38]), yielding the plasmids pAR410–cJun and pAR410–$JunW_{Ph1}$.

BL21 cells were chemically cotransformed with the plasmids pREP4, pAR300–cFos–DHFR2 (described in Mason *et al.*[37]), and pAR200–*helix*–DHFR1, where *helix* stands for $JunW_{Ph1}$, $JunW_{Ph2}$, JunW, or cJun. Cells were plated on LB agar plates containing 50 μg/ml kanamycin, 100 μg/ml ampicillin, and 25 μg/ml chloramphenicol. Single clones were picked and grown overnight in M9 minimal medium with the same antibiotics. Subsequently, the culture was diluted to an OD_{600} of 0.006 in a total volume of 20 ml M9 medium. For selective pressure, 1 μg/ml trimethoprim was added and cells were induced with 1 mM IPTG to express the DHFR fusion proteins. As control, additional cultures were grown in the absence of IPTG. A triplicate of each sample was measured at OD_{600} every 2 h to monitor growth. For competitive growth

assays, cells with respective plasmids (see above) were transformed with either one of the plasmids pAR410–cJun, pAR410–JunW$_{Ph1}$, or pAR410–mock. Growth assays were performed as described above.

SDS-PAGE and Western blot analysis

For detection of JunWinner–DHFR1 fragments, cultures were grown under selective conditions and harvested in the exponential phase. OD_{600} was determined for all samples, and 10 μl of an equivalence of $OD_{600}=2$ was loaded onto an SDS polyacrylamide gel (12.5%) and run for 1.5 h at 120 V. Protein samples were either stained with Coomassie (Serva) or transferred (30 min at 120 V) to a nitrocellulose membrane (Hybond ECL, GE Healthcare), which had been soaked in 50 mM Tris, 150 mM glycine, and 10% (v/v) methanol, pH 8.3. The membrane was blocked with milk powder (3% w/v, TBS, 4 °C) and washed three times for 5 min (TBS, room temperature). DHFR fragments were detected by incubation with a 1:1600 dilution of an anti-His antibody coupled to horseradish peroxidase (Sigma) in TBS with 0.1% (w/v) BSA (Sigma) and 0.05% Tween (Sigma) for 1 h at room temperature. The membrane was washed three times for 5 min with TBS containing 0.1% Tween. The membrane was stained with Fast DAB peroxidase substrate (Sigma). The reaction was stopped by washing with water. Molecular weight markers were PageRuler, unstained (Fermentas) for SDS-PAGE and Prestained Protein Marker, Broad Range (NEB) for Western Blots. The band intensity from Coomassie-stained SDS gels was determined using Quantity One software (Bio-Rad Laboratories). The ratio between the DHFR fragments and three different background proteins was calculated independently. Values were normalized and the average was determined.

Construction, expression, and purification of *helix*–GFP fusion proteins

GFP fusions were used to ease expression and detection and to be able to directly transfer data to future *in vivo* experiments. The GFP gene was amplified via PCR out of the pEGFP vector (Clontech) with overlapping primers that carry an AscI/SpeI site and a HindIII site (underlined) (forward: 5′-ATAACCGGCGCGCCAGGTCGTAAGAAACGCCGTCAACGTCGTCGCTCAGGTAGCTCTGGCACTTCAAGCGGTACTAGTATGGTGAGCAAGGGCGAG-3′; reverse: 5′-ATAACCAAGCTTTCATTACTTGTACAGCTCGTCCA-3′). The PCR product was digested with SpeI/HindIII and ligated into the vector pAR200–JunW–DHFR1[37] from which the DHFR1 fragment had been removed using the same enzymes, resulting in the vector pAR200–*helix*–GFP. The inserts for *helix* JunW$_{Ph1}$, JunW$_{Ph2}$, JunW, cJun, and cFos were subcloned via NheI/AscI digest from the corresponding phage vectors or out of the GSTcFos vector into pAR200–*helix*–GFP. A short mock peptide sequence (coding for Val, Lys, and Ser) served as negative control. All vectors encode an N-terminal 6× histidine tag for affinity IMAC purification.

Plasmids encoding the 6×His–helix–GFP fusion proteins were transformed into BL21 (Stratagene) containing pREP4 (Qiagen). A preculture was grown at 26 °C overnight in 2YT medium (100 μg/ml ampicillin and 50 μg/ml kanamycin). The preculture was diluted to an OD_{600} of 0.1 and induced (1 mM IPTG) at an OD_{600} of 0.5–0.6. Cells were harvested after 8–10 h growth at 26 °C and resuspended in lysis buffer (50 mM NaH_2PO_4, 300 mM NaCl, and 10 mM imidazole, pH 8). Cells were lysed by sonication on ice, and cell debris was spun down at 19,000*g* at 4 °C for 30 min. The supernatant was immediately loaded onto a Ni-NTA affinity column (Qiagen), washed with 240 ml washing buffer (50 mM NaH_2PO_4, 300 mM NaCl, and 40 mM imidazole, pH 8), and eluted with elution buffer (50 mM NaH_2PO_4, 300 mM NaCl, and 250 mM imidazole, pH 8). The eluted volume was concentrated to 1 ml using a Vivaspin column with a molecular mass cutoff <14 kDa. For further purification, samples were injected on a size-exclusion column (Superdex 200, GE Healthcare) using 10 mM Hepes, pH 7.6, 150 mM NaCl, and 1 mM ethylenediaminetetraacetic acid (EDTA) as running buffer and a flow rate of 0.5 ml/min. Concentrations of the purified proteins were determined from absorbance spectra measurements at 280 nm.

Cloning of basic-cJun and basic-cFos targets

The genes encoding the basic-cFos and the basic-cJun domains were cloned via PCR using the following primers: (a) basic-cJunT: forward, 5′-GCAATAGCTAGCCGCATTAAAGCCGAACGCAAACGGATGCGCAACCGCATCGCAGCCTCCAAGTGCCGCAAACGCAAATTGGAGCGCATCGCCCGCTTGG-3′; reverse, 5′-GCAATAAGGCGCGCCGAGCTGGGCCACCTGTTCGCG CAACATGTTG GCGGTGGAGG CCAGCTCATA GTTCTGTGCT TTCAGGGTTTTCACCTTTTCTTCCAAGCGGGCGATGCGCTCC-3′; (b) basic-cFosT: forward, 5′-GCAATAGCTAGCGAGGAAAAACGCCGCATCCGGCGTGAACGCAACAAAATGGCCGCGGCGAAGTGCCGCAACCGCCGTCGGGAACTGACCGATACCTTGCAGGCCG-3′; reverse, 5′-GCAATAAGGCGCGCCCAGTTTCTCCTTTTCTTTAAGCAGGTTTGCGATTTCGGTCTGGAGGGCATATTTTTCATCTTCAAGCTGATCGGTCT CGGCCTGCAAGGTATCGGTCAG-3′. The PCR product was subsequently digested with NheI/AscI (underlined) and ligated into pAR200–*helix*–GFP, which was digested with the same enzymes, resulting in pAR200–basic-cFos–GFP and pAR200–basic-cJun–GFP.

Both constructs carry an N-terminal 6× histidine tag for affinity IMAC purification. The protein expression and purification were performed as described in the section above. The cloning and purification of the basic-Myc and basic-Max proteins, which were kindly provided by E.M. Jouaux, are detailed in Jouaux *et al.*[51]

Determination of the oligomerization state

The oligomerization state was assessed by SEC experiments. A standard curve was derived using a set of marker proteins [aldolase (158 kDa, Sigma), BSA (67 kDa, Sigma), catalase (232 kDa, Sigma), chymotrypsin (23.6 kDa, Sigma), RNase (13.7 kDa, Sigma), ovalbumin (43 kDa, Sigma), vitamin B_{12} (Sigma), and dextran blue (Serva)]. Interacting complexes were mixed at a concentration of 20 μM and a flow rate of 0.5 ml/min. The molecular weights of the examined complexes were calculated from the standard curve.

Peptide synthesis and CD measurement

Peptides (sequences are shown in Table 1) were synthesized with an N-cap (AS) and C-cap (GAP) sequence and acetylated N- and amidated C-terminus by Protein Peptide Research (Wickham, UK). Peptides were purified to >98% purity by reversed-phase HPLC using a Jupiter Proteo column (4 μm particle size, 90 Å pore size, 250×10

mm, Phenomenex) and a gradient of 20–60% acetonitrile (0.1% trifluoric acid) in 40 min at 1 ml/min. Correct masses were determined by in-house electrospray mass spectrometry. Peptide concentrations were determined in water by using absorbance at 280 nm with an extinction coefficient of 1209 M^{-1} cm^{-1} corresponding to a Tyr residue inserted at position **b3**.

Peptide solutions were mixed to a concentration of 150 μM total peptide in CD buffer (10 mM potassium phosphate and 100 mM KF, pH 7.0). CD measurements were carried out in a Jasco J-810 spectropolarimeter. Spectra were recorded at 5 °C and 20 °C. Thermal denaturation was recorded at 222 nm from −8 °C to 96 °C with a gradient of 30 °C/h to monitor unfolding of the coiled coil. The path length of the cuvette was 1 mm for all measurements. The thermal denaturation data were globally fitted to a two-state model[37] to yield the T_m of the respective complexes (Fig. 4). The transitions of the mutant $JunW_{E23K}$ were approximated by calculating fraction unfolded and using the first derivative.

Dissociation constants (Fig. 7) were derived from heat denaturation profiles by calculating K_d values from fraction folded and unfolded within the transition region and linear extrapolation to the reference temperature. To account for inaccuracies due to the temperature dependence of ΔH, we used an empirical correlation between K_d values derived from temperature denaturation [K_d(temp)] *versus* K_d values derived from urea denaturation [K_d(urea)]:

$$\ln K_d(\text{temp}) = 1.1982 \times \ln K_d(\text{urea}) + 0.3222; r^2 = 0.9957 \quad (2)$$

This correlation was obtained by relating measured K_d (urea, 20 °C) values with calculated K_d(temp) values for nine different coiled coils.[23,37]

Prediction of coiled-coil interaction

A previously developed algorithm, bCIPA‡,[37] was modified by including the presented data as well as other data from the lab.[38] The algorithm uses matrices for **a**/**a** and **d**/**d** C, **g**/**e** ES, and HP to predict T_m values according to the following equation:

$$T_m = a_1 \times \text{HP} + a_2 \times \text{C} + a_1 \times \text{ES} + d \quad (3)$$

Using adjusted C (II ~ LL ~ VI = −1.5; VV ~ VL ~ IL ~ IR ~ IK = −1.0; IA ~ LA ~ VA ~ NN ~ IN ~ IT ~ LK ~ LT ~ RR = −0.5; VT = +0.5) and ES matrices (RE = −2; KE ~ KQ ~ RQ ~ QQ = −1.5; QE = −1.0; QA ~ RA ~ KD ~ RD ~ KL ~ TL ~ RK = −0.5; EE ~ KK ~ RR = +0.5; DD ~ DE ~ TR = +1.0) as well as the previously used HP scale,[52] we fitted measured T_m values of all Jun and Fos variants as well as WinZip peptides[23] and obtained the following coefficients: $a_1 = 81.3256$, $a_2 = -10.5716$, $a_3 = -4.7771$, and $d = -29.1320$. At first glance, these coefficients seem to be very different. However, this is explained by the differences of the three scoring matrices for HP, C, and ES resulting in different values for the most and least stable pairs: The pairs with the highest and lowest core ranking have C scores of −14 (best) and −8 (worst), respectively, resulting in a difference of −6 between the best and the worst pair. The pairs with the highest and lowest electrostatic ranking have ES scores of −10 (best) and +3 (worst), respectively, resulting in a difference of −13. The pairs with the highest and lowest HP display HP scores of 2.6237 (best) and 2.2600 (worst), resulting in a difference of 0.3637. If these differences are multiplied with their respective coefficients, a_1, a_2, and a_3, the resulting values for C, ES, and HP are +63, +62, and +30, respectively, indicating that they are all in the same range and, therefore, have similar weights, with a slight emphasis on C and ES compared to HP.

‡ www.molbiotech.uni-freiburg.de/bCIPA

Electrophoretic mobility shift assay

Purified basic-cFos–GFP (MW = 36 kDa) and basic-cJun–GFP (MW = 36 kDa) proteins were mixed in a 1:1 ratio of either 50 or 100 ng of each protein and added to the AP-1 DNA recognition sequence (5′-GTCAGTCAGTGACTCAATCGGTCA-3′, TRE underlined). The E-box DNA (5′-GTCAGTCAGCCACGTGATCGGTCA-3′, E-box underlined) served as negative control. Basic-Myc and basic-Max proteins (bHLHZip domains; kindly provided by E.M. Jouaux[51]) were mixed in a 1:1 ratio and added to the E-box DNA in the presence of the selected peptides or cJun to test for unspecific binding. The DNA was labeled with ^{32}P-γ-ATP and diluted to 5000 Cherenkov counts/μl. Purified cJun–, $JunW_{Ph1}$–, $JunW_{Ph2}$–, and JunW–GFP fusion proteins or a mock control peptide were incubated with the target proteins and 1 μl labeled DNA for 30 min on ice in reaction buffer [0.25 μl 50 μg/μl BSA, 10 μl 2× BS buffer, 1 μl 0.5 μg/μl poly(dI–dC), 0.1 μl 1 M DTT, 1.2 μl 1% NP40, H_2O ad 20 μl, with 2× BS buffer: 20 mM Hepes, 120 mM KCl, 8% Ficoll, 2 mM EDTA, 10 mM $MgCl_2$, pH 7.9]. Inhibitors were added in 2-fold or 20-fold excess either directly or 15 min after preincubation of the Jun:Fos:DNA complex. The binding complexes were resolved on a native 6% polyacrylamide gel (30%/0.8%) in 0.5× TBE buffer (taken from a 10× stock solution: 1 M Tris, 1 M boric acid, and 25 mM EDTA) and visualized from dried gels using a PharosFX Plus Molecular Imager (Bio-Rad Laboratories).

Acknowledgements

We thank Eva Jouaux for kindly providing Myc and Max peptides for EMSA experiments; Karin Schmidtkunz, Josefine Tadewaldt, and Annette Gaida for excellent experimental assistance; and Tobias J. Erb from the laboratory of Prof. G. Fuchs for kindly providing the calibration proteins for SEC. This work was funded by the Emmy-Noether program of the Deutsche Forschungsgemeinschaft (Grant Ar 373/1-1 and 1-2).

Supplementary Data

Supplementary data associated with this article can be found, in the online version, at doi:10.1016/j.jmb.2008.04.030

References

1. Maki, Y., Bos, T. J., Davis, C., Starbuck, M. & Vogt, P. K. (1987). Avian sarcoma virus 17 carries the jun oncogene. *Proc. Natl Acad. Sci. USA*, **84**, 2848–2852.

2. van Straaten, F., Müller, R., Curran, T., Van Beveren, C. & Verma, I. M. (1983). Complete nucleotide sequence of a human c-onc gene: deduced amino acid sequence of the human c-fos protein. *Proc. Natl Acad. Sci. USA*, **80**, 3183–3187.
3. Grigoriadis, A. E., Schellander, K., Wang, Z. Q. & Wagner, E. F. (1993). Osteoblasts are target cells for transformation in c-fos transgenic mice. *J. Cell Biol.* **122**, 685–701.
4. Young, M. R., Li, J. J., Rincon, M., Flavell, R. A., Sathyanarayana, B. K., Hunziker, R. & Colburn, N. (1999). Transgenic mice demonstrate AP-1 (activator protein-1) transactivation is required for tumor promotion. *Proc. Natl Acad. Sci. USA*, **96**, 9827–9832.
5. Eferl, R., Ricci, R., Kenner, L., Zenz, R., David, J. P., Rath, M. & Wagner, E. F. (2003). Liver tumor development. c-Jun antagonizes the proapoptotic activity of p53. *Cell*, **112**, 181–192.
6. Chinenov, Y. & Kerppola, T. K. (2001). Close encounters of many kinds: Fos–Jun interactions that mediate transcription regulatory specificity. *Oncogene*, **20**, 2438–2452.
7. Shaulian, E. & Karin, M. (2002). AP-1 as a regulator of cell life and death. *Nat. Cell Biol.* **4**, E131–E136.
8. Glover, J. N. & Harrison, S. C. (1995). Crystal structure of the heterodimeric bZIP transcription factor c-Fos–c-Jun bound to DNA. *Nature*, **373**, 257–261.
9. John, M., Briand, J. P., Granger-Schnarr, M. & Schnarr, M. (1994). Two pairs of oppositely charged amino acids from Jun and Fos confer heterodimerization to GCN4 leucine zipper. *J. Biol. Chem.* **269**, 16247–16253.
10. Junius, F. K., O'Donoghue, S. I., Nilges, M., Weiss, A. S. & King, G. F. (1996). High resolution NMR solution structure of the leucine zipper domain of the c-Jun homodimer. *J. Biol. Chem.* **271**, 13663–13667.
11. O'Shea, E. K., Rutkowski, R. & Kim, P. S. (1992). Mechanism of specificity in the Fos–Jun oncoprotein heterodimer. *Cell*, **68**, 699–708.
12. Crick, F. H. (1953). The packing of alpha-helices: simple coiled-coils. *Acta Crystallogr., Sect. A*, **6**, 689–697.
13. Lupas, A. N. & Gruber, M. (2005). The structure of alpha-helical coiled coils. *Adv. Protein Chem.* **70**, 37–78.
14. Mason, J. M., Müller, K. M. & Arndt, K. M. (2007). Considerations in the design and optimization of coiled coil structures. *Methods Mol. Biol.* **352**, 35–70.
15. Woolfson, D. N. (2005). The design of coiled-coil structures and assemblies. *Adv. Protein Chem.* **70**, 79–112.
16. Wagschal, K., Tripet, B., Lavigne, P., Mant, C. & Hodges, R. S. (1999). The role of position a in determining the stability and oligomerization state of alpha-helical coiled coils: 20 amino acid stability coefficients in the hydrophobic core of proteins. *Protein Sci.* **8**, 2312–2329.
17. Tripet, B., Wagschal, K., Lavigne, P., Mant, C. T. & Hodges, R. S. (2000). Effects of side-chain characteristics on stability and oligomerization state of a *de novo*-designed model coiled-coil: 20 amino acid substitutions in position "d". *J. Mol. Biol.* **300**, 377–402.
18. Krylov, D., Mikhailenko, I. & Vinson, C. (1994). A thermodynamic scale for leucine zipper stability and dimerization specificity: e and g interhelical interactions. *EMBO J.* **13**, 2849–2861.
19. Krylov, D., Barchi, J. & Vinson, C. (1998). Inter-helical interactions in the leucine zipper coiled coil dimer: pH and salt dependence of coupling energy between charged amino acids. *J. Mol. Biol.* **279**, 959–972.
20. Acharya, A., Rishi, V. & Vinson, C. (2006). Stability of 100 homo and heterotypic coiled-coil a–a′ pairs for ten amino acids (A, L, I, V, N, K, S, T, E, and R). *Biochemistry*, **45**, 11324–11332.
21. Acharya, A., Ruvinov, S. B., Gal, J., Moll, J. R. & Vinson, C. (2002). A heterodimerizing leucine zipper coiled coil system for examining the specificity of a position interactions: amino acids I, V, L, N, A, and K. *Biochemistry*, **41**, 14122–14131.
22. Mason, J. M. & Arndt, K. M. (2004). Coiled coil domains: stability, specificity, and biological implications. *ChemBioChem*, **5**, 170–176.
23. Arndt, K. M., Pelletier, J. N., Müller, K. M., Plückthun, A. & Alber, T. (2002). Comparison of *in vivo* selection and rational design of heterodimeric coiled coils. *Structure*, **10**, 1235–1248.
24. O'Shea, E. K., Lumb, K. J. & Kim, P. S. (1993). Peptide 'Velcro': design of a heterodimeric coiled coil. *Curr. Biol.* **3**, 658–667.
25. Graddis, T. J., Myszka, D. G. & Chaiken, I. M. (1993). Controlled formation of model homo- and heterodimer coiled coil polypeptides. *Biochemistry*, **32**, 12664–12671.
26. Nautiyal, S. & Alber, T. (1999). Crystal structure of a designed, thermostable, heterotrimeric coiled coil. *Protein Sci.* **8**, 84–90.
27. Nautiyal, S., Woolfson, D. N., King, D. S. & Alber, T. (1995). A designed heterotrimeric coiled coil. *Biochemistry*, **34**, 11645–11651.
28. Beck, K., Dixon, T. W., Engel, J. & Parry, D. A. (1993). Ionic interactions in the coiled-coil domain of laminin determine the specificity of chain assembly. *J. Mol. Biol.* **231**, 311–323.
29. Nomizu, M., Utani, A., Beck, K., Otaka, A., Roller, P. P. & Yamada, Y. (1996). Mechanism of laminin chain assembly into a triple-stranded coiled-coil structure. *Biochemistry*, **35**, 2885–2893.
30. Zeng, X., Zhu, H., Lashuel, H. A. & Hu, J. C. (1997). Oligomerization properties of GCN4 leucine zipper e and g position mutants. *Protein Sci.* **6**, 2218–2226.
31. Pu, W. T. & Struhl, K. (1993). Dimerization of leucine zippers analyzed by random selection. *Nucleic Acids Res.* **21**, 4348–4355.
32. Sharma, V. A., Logan, J., King, D. S., White, R. & Alber, T. (1998). Sequence-based design of a peptide probe for the APC tumor suppressor protein. *Curr. Biol.* **8**, 823–830.
33. Arndt, K. M., Pelletier, J. N., Müller, K. M., Alber, T., Michnick, S. W. & Plückthun, A. (2000). A heterodimeric coiled-coil peptide pair selected *in vivo* from a designed library-*versus*-library ensemble. *J. Mol. Biol.* **295**, 627–639.
34. Olive, M., Krylov, D., Echlin, D. R., Gardner, K., Taparowsky, E. & Vinson, C. (1997). A dominant negative to activation protein-1 (AP1) that abolishes DNA binding and inhibits oncogenesis. *J. Biol. Chem.* **272**, 18586–18594.
35. Mathas, S., Hinz, M., Anagnostopoulos, I., Krappmann, D., Lietz, A., Jundt, F. *et al.* (2002). Aberrantly expressed c-Jun and JunB are a hallmark of Hodgkin lymphoma cells, stimulate proliferation and synergize with NF-kappa B. *EMBO J.* **21**, 4104–4113.
36. Pelletier, J. N., Arndt, K. M., Plückthun, A. & Michnick, S. W. (1999). An *in vivo* library-*versus*-library selection of optimized protein–protein interactions. *Nat. Biotechnol.* **17**, 683–690.
37. Mason, J. M., Schmitz, M. A., Müller, K. M. & Arndt, K. M. (2006). Semirational design of Jun–Fos coiled coils with increased affinity: universal implications for leucine zipper prediction and design. *Proc. Natl Acad. Sci. USA*, **103**, 8989–8994.

38. Mason, J. M., Müller, K. M. & Arndt, K. M. (2007). Positive aspects of negative design: simultaneous selection of specificity and stability. *Biochemistry*, **46**, 4804–4814.
39. Cooper, T. M. & Woody, R. W. (1990). The effect of conformation on the CD of interacting helices: a theoretical study of tropomyosin. *Biopolymers*, **30**, 657–676.
40. Lau, S. Y., Taneja, A. K. & Hodges, R. S. (1984). Synthesis of a model protein of defined secondary and quaternary structure. Effect of chain length on the stabilization and formation of two-stranded alpha-helical coiled-coils. *J. Biol. Chem.* **259**, 13253–13261.
41. Newman, J. R. & Keating, A. E. (2003). Comprehensive identification of human bZIP interactions with coiled-coil arrays. *Science*, **300**, 2097–2101.
42. Willemsen, T., Hagemann, U. B., Jouaux, E. M., Stebel, S. C., Mason, J. M., Müller, K. M. & Arndt, K. M. (in press). Protein engineering. In *Protein and Cell Biomethods Handbook* (Rapley, R. & Walker, J., eds), 2nd edit., Humana Press.
43. Lai, J. R., Fisk, J. D., Weisblum, B. & Gellman, S. H. (2004). Hydrophobic core repacking in a coiled-coil dimer via phage display: insights into plasticity and specificity at a protein–protein interface. *J. Am. Chem. Soc.* **126**, 10514–10515.
44. Zhu, H., Celinski, S. A., Scholtz, J. M. & Hu, J. C. (2001). An engineered leucine zipper a position mutant with an unusual three-state unfolding pathway. *Protein Sci.* **10**, 24–33.
45. Mason, J. M., Hagemann, U. B. & Arndt, K. M. (2007). Improved stability of the Jun–Fos Activator Protein-1 coiled coil motif: a stopped-flow circular dichroism kinetic analysis. *J. Biol. Chem.* **282**, 23015–23024.
46. Krylov, D., Olive, M. & Vinson, C. (1995). Extending dimerization interfaces: the bZIP basic region can form a coiled coil. *EMBO J.* **14**, 5329–5337.
47. Krylov, D., Kasai, K., Echlin, D. R., Taparowsky, E. J., Arnheiter, H. & Vinson, C. (1997). A general method to design dominant negatives to B-HLHZip proteins that abolish DNA binding. *Proc. Natl Acad. Sci. USA*, **94**, 12274–12279.
48. Porte, D., Oertel-Buchheit, P., John, M., Granger-Schnarr, M. & Schnarr, M. (1997). DNA binding and transactivation properties of Fos variants with homodimerization capacity. *Nucleic Acids Res.* **25**, 3026–3033.
49. Fong, J. H., Keating, A. E. & Singh, M. (2004). Predicting specificity in bZIP coiled-coil protein interactions. *Genome Biol.* **5**, R11.
50. Day, L. A. (1969). Conformations of single-stranded DNA and coat protein in fd bacteriophage as revealed by ultraviolet absorption spectroscopy. *J. Mol. Biol.* **39**, 265–277.
51. Jouaux, E. M., Schmidtkunz, K., Müller, K. M. & Arndt K. M. (2008). Targeting the c-Myc coiled coil with interfering peptides. *J. Pept. Sci.* In the press. doi:10.1002/psc.1038.
52. Williams, R. W., Chang, A., Juretic, D. & Loughran, S. (1987). Secondary structure predictions and medium range interactions. *Biochim. Biophys. Acta*, **916**, 200–204.